SCIENCE CHINA
Information Sciences

• Supplementary File •

High-sensitivity Piezoelectric Composite Ultrasonic Transducers Based on Fresnel Lenses for High-Resolution Imaging

Zhaoxi Li[1,2,†], Yiheng Yang[1,†], Chenxue Hou[1], Xiongwei Wei[1], Yi Quan[1], Xiaozhou Lü[2], Chunlong Fei[1,*], Weimin Bao[2] & Yintang Yang[1,*]

[1]*School of Microelectronics, Xidian University, Xi'an 710071, China*
[2]*School of Aerospace Science and Technology, Xidian University, Xi'an 710071, China*

Appendix A The 1 - 3 - 2 Piezoelectric Composite material

Appendix A.1 Structural Configurations of 1-3-2 and 1-3 Composite Types

The structure of 1-3 piezoelectric composites consists of 1D piezoelectric rods arranged parallelly in a 3D polymer, thereby enhancing the longitudinal thickness electromechanical coupling coefficient [1, 2]. As shown in **Figure A1**, the 1-3-2 piezoelectric composite material is formed by connecting the conventional 1-3 composite material in series with a ceramic substrate along the ceramic polarization direction [3]. This enhancement not only stabilizes mechanical performance but also provides a high thickness electromechanical coupling coefficient (often >0.6). The higher the coupling coefficient, the better the energy conversion between electrical energy and mechanical energy. Therefore, the 1-3-2 piezoelectric composite material can effectively improve the transmission efficiency, sensitivity and robustness of ultrasound transducers in underwater applications [4].

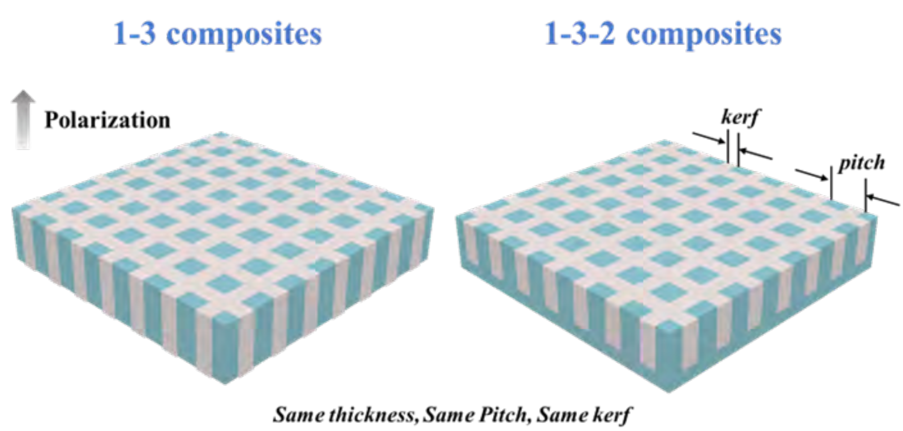

Figure A1 Comparative structural diagram of 1-3-2 and 1-3 composite materials.

Appendix A.2 The Theoretical Derivations and Parameter Selections

The equivalent piezoelectric, dielectric and elastic properties of 1-3-2 piezoelectric composite material are derived as follows:

$$
\begin{aligned}
c^E_{33(1-3-2)} &= \mathbf{c}^E_{33}(M_1 c^E_{33} + M_2 e_{33}) - e_{33(1-3)}(-M_2 c^E_{33} + M_3 e_{33}) \\
e_{33(1-3-2)} &= e_{33(1-3)}(M_1 c^E_{33} + M_2 e_{33}) + \varepsilon^S_{33(1-3)}(-M_2 c^E_{33} + M_3 e_{33}) \\
\varepsilon_{33(1-3-2)} &= e_{33(1-3)}(-M_1 e^E_{33} + M_2 \varepsilon^S_{33}) + \varepsilon^S_{33(1-3)}(M_2 e_{33} + M_3 \varepsilon^S_{33})
\end{aligned}
\tag{A1}
$$

$$
\begin{aligned}
M_1 &= \frac{(1+t)(\varepsilon^S_{33(1-3)} + t\varepsilon^S_{33})}{N}, M_2 = \frac{(1+t)(e_{33(1-3)} + te_{33})}{N}, M_3 = \frac{(1+t)(c^E_{33(1-3)} + tc^E_{33})}{N} \\
N &= ((\varepsilon^S_{33(1-3)} + t\varepsilon^S_{33})(c^E_{33(1-3)} + tc^E_{33}) + (e_{33(1-3)} + te_{33}))^2
\end{aligned}
\tag{A2}
$$

* Corresponding author (email: clfei@xidian.edu.cn, ytyang@xidian.edu.cn)
† Equally contributed to this work.

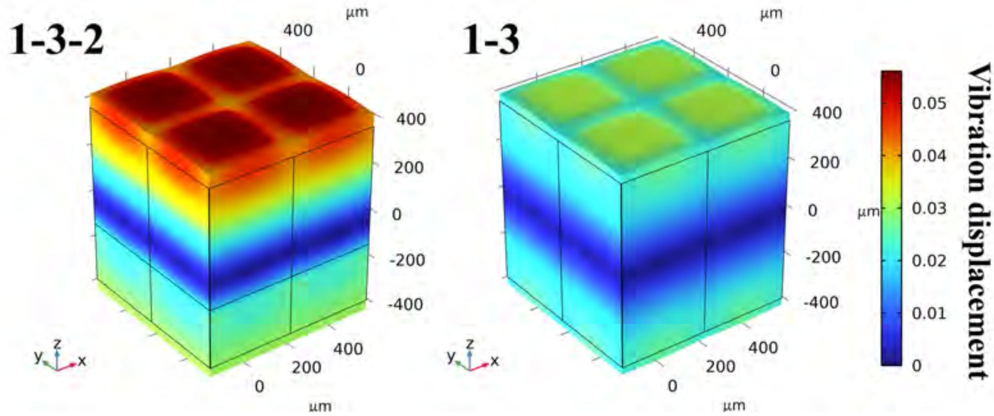

Figure A2 Comparison of displacement variables of vibration modes for 1-3-2 and 1-3 composite materials.

Among them, c_{33}^E, c_{33}^D, ε_{33}^S, e_{33} are the elastic constant, dielectric constant and piezoelectric constant of 1-3 composites, respectively. According to the above equivalent calculation, the equivalent density(ρ), electromechanical coupling coefficient(k_t) and equivalent acoustic impedance (Z) of 1-3-2 composites can be further calculated:

$$\rho_{1-3-2} = \rho_p V_1 + \rho_m (1 - V_1), \quad k_t = \sqrt{1 - \frac{c_{33(1-3-2)}^E}{\mathbf{c}_{33(1-3-2)}^D}}, \quad Z = \sqrt{c_{33(1-3-2)}^D \times \rho_{(1-3-2)}} \tag{A3}$$

$$\mathbf{c}_{33(1-3-2)}^D = c_{33(1-3-2)}^E + \frac{e_{33(1-3-2)}^2}{\varepsilon_{33(1-3-2)}^S} \tag{A4}$$

The relationship between Z, k_t and piezoelectric phase volume fraction of 1-3-2 composite is shown in **Figure A3 (b)**. In order to take into account its high voltage electrical characteristics and low acoustic impedance characteristics, the volume ratio of the composite piezoelectric element is 0.603. Then, 1-3-2 piezoelectric composite material was prepared by cutting and filling method. The preparation process mainly includes grinding, polishing and cutting of piezoelectric material (PZT-5H), epoxy perfusion, etc. Finally, a piezoelectric composite material with a diameter of 25 mm and a thickness of 750 μm piezoelectric layer was prepared, and epoxy was poured as the backing layer and fixed filling. The corresponding material functions and acoustic parameters are shown in **Table A1**. In addition, the impedance spectrum measurement results of the transducer measured by the impedance analyzer (WK6500B 1J65120B, Wayne Kerr Electronics, UK) are shown in **Figure A3 (c)**. The resonant frequency fr and the anti-resonant frequency fa are obtained from the impedance spectrum respectively, and the equivalent electromechanical coupling coefficient is calculated according to Formula 5. After calculation, the center frequency of the transducer is 2.2 MHz and k_{teff} is 0.64.

$$k_{teff} = \sqrt{\frac{\pi}{2} \times \frac{f_r}{f_a} \times \tan\left(\frac{\pi(f_a - f_r)}{2f_a}\right)} \tag{A5}$$

Table A1 Design parameters of the transducer

Material	Function	c (m/s)	ρ (kg/m^3)	Z_α (Mrayl)
PZT - 5H	1 - 3 composite piezoelectric material	4200	7500	31.50
Filled Epoxy	1 - 3 composite polymer material	2450	1100	2.69
Water	Front - load	1540	1000	1.54
Backing Epoxy	Backing	2400	1200	2.88

Appendix B The Fresnel Lens Theory and Design

Appendix B.1 Fresnel Lens Theory and Calculation

Each annular Fresnel zone provides phase compensation for the acoustic waves passing through it, making the phases of all acoustic waves passing through the lens consistent at the focal point, thus achieving acoustic wave focusing. Fresnel lenses achieve focusing by controlling the height(h) and radius(r_n) between the rings, with each pair of steps having the same height difference [5,6]:

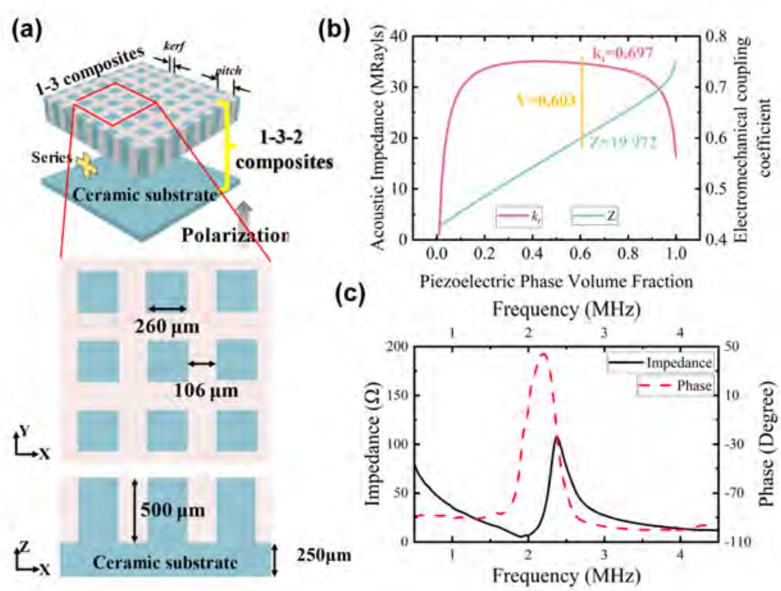

Figure A3 (a) The front view and side view of the 1-3-2 composite structure; (b) the relationship between equivalent acoustic impedance, electromechanical coupling coefficient and piezoelectric phase volume fraction of 1-3-2 composite; (c) the impedance spectrum measured results.

$$h = \left[Kf \left(\frac{1}{v_l} - \frac{1}{v_s} \right) \right]^{-1}$$
$$r_n = \sqrt{\left(F + \frac{n\lambda}{K} \right)^2 - F^2} \tag{B1}$$

Where v_l is the speed of sound in liquid, v_s is the speed of sound in the lens material, taken as 2400 m/s, f is the central frequency, K is the Fresnel order, The radius of each ring is:

$$v_n = \sqrt{\left(F + \frac{n\lambda}{K} \right)^2 - F^2} \tag{B2}$$

n is the order number of the Fresnel zone, n=1,2,3 ..., and F stands for focal length. In the field of acoustic applications, the selection of parameters for acoustic Fresnel lenses has a significant impact on the performance of ultrasonic imaging and focusing systems. Among these parameters, the Fresnel order is a crucial one. The working principle of acoustic Fresnel lens is based on the principle of acoustic wavefront propagation. The Fresnel order (K) determines the number of phase - shifting regions in the lens and the magnitude of the phase shift. For instance, in a circular acoustic Fresnel lens, the phase difference between two adjacent orders is $\Delta\varphi = 2\pi/K$.

At the same time, different operating frequencies will also affect the choice of Fresnel order. Within a certain range, the higher the design frequency and the more orders of the Fresnel lens, the higher the lateral resolution of its modulated focused sound beam. However, high working frequencies and Fresnel orders will reduce the characteristic size of the lens and require higher precision, which greatly increases the complexity and difficulty of the preparation process. Therefore, low-order lenses (K=2, 3) are often selected for high-frequency situations, mainly considering the situation where the focusing requirements are not high but the precision is limited. Medium-order lenses (K=4, 5, 6) are aimed at the tradeoff between focusing performance and system. High-order situations ($K \geqslant 7$) are mainly used for high resolution and close focal length situations.

Appendix B.2 The Specific Design and Preparation Process

Fresnel lenses are prepared through 3D printing based on the above theory. In this work we designed and fabricated 6 Fresnel lenses with orders 4, 6 and 8 and focal lengths of 25 mm and 50 mm respectively. The material used is GR rigid resin (sound speed is 2400 m/s and density is 1300 kg/m^3), which achieves efficient transmission and modulation. In the manufacturing process, first of all, according to the design theory of Fresnel lenses, professional 3D modeling software SolidWorks is used to design lens models of different orders (fourth order, sixth order, and eighth order) and different focal lengths (25 mm and 50 mm). Then, these models were imported into a 3D printer, and high-precision printing parameters (printing resolution of 50 μm) were set to ensure the dimensional accuracy and surface quality of the lenses.

For impedance matching considerations, a 1 mm thick lens substrate is reserved to act as an impedance matching layer, according to the quarter-wavelength matching layer design theory. Two different focal lengths were chosen to evaluate different $f_{\#}$ values (defined as the ratio of focal length to lens diameter) and characterize their impact on the performance of the ultrasonic transducer. **Figure B1** shows a schematic diagram of the fourth-order Fresnel lens structure, which has a series of concentric rings to change the phase distribution, thereby achieving effective acoustic beam focusing. **Figure B2** shows the efficient focusing using a Fresnel lens compared to a flat acoustic source.

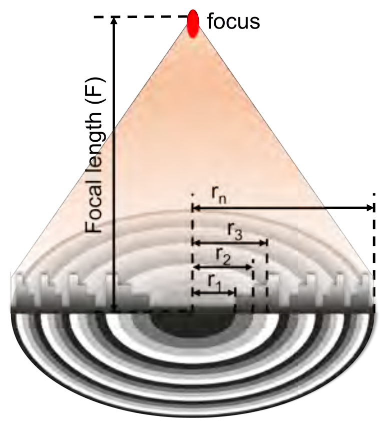

Figure B1 Schematic diagram of the Fresnel lens structure and focusing.

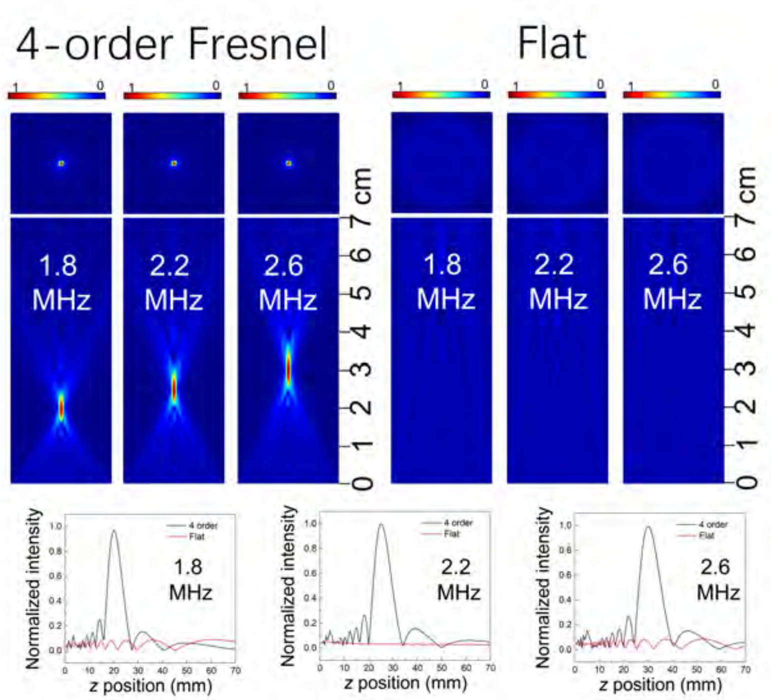

Figure B2 Acoustic field intensity maps of Fresnel lenses and a flat acoustic source (without lens) at frequencies ranging from 1.8 to 2.6 MHz.

Appendix C Experiment and Comparison

Appendix C.1 Acoustic Field-Testing Setup

The ultrasonic transducer is driven by an AFG 3251 function generator and an ATA-122D power amplifier to transmit electrical signals. A needle hydrophone was placed at the bottom of a tank filled with deionized water. Surface acoustic field 2D scanning was performed using a computer-controlled 3D motion system with a step size of 50 μm. The signal received by the hydrophone (NH1000, PA, UK) is sampled by the QT 1140 acquisition card and transmitted to the computer for processing. The schematic diagram of the motion scanning acquisition system and experimental setup is shown in **Figure**

C1. The time delay spectrum method [7] is used to calibrate the needle hydrophone in the frequency range from 1.2 MHz to 3.0 MHz. Finally, the three-dimensional reconstruction of the acoustic field was performed to generate the 3D acoustic pressure distribution through MATLAB software.

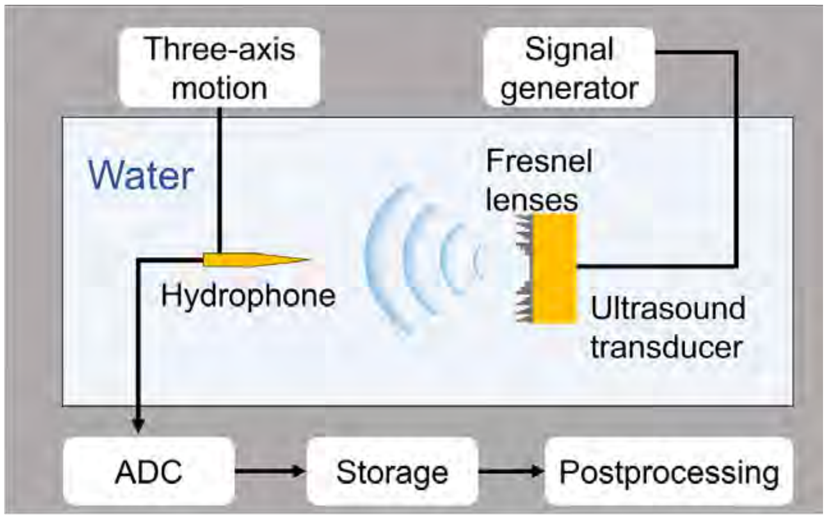

Figure C1 Schematic diagram of the motor control system and the device under test.

Appendix C.2 Experimental Acoustic Field Testing

To better characterize the broadband focusing capability, we provide the changes in focal length at different frequencies in **Figure C3 (a)** and **(b)**. The self-focusing mode can be intuitively observed according to the focal length curve: as the excitation frequency increases, the focal spot gradually moves away from the lens surface, showing a linear relationship with frequency in the range of 1.2 MHz to 3.0 MHz, and the focal length change is basically consistent with the simulation results. In addition, the lateral acoustic pressure distribution of different orders and focal lengths at the center frequency of 2.2 MHz is shown in **Figure C3 (c)-(e)**. It is obvious that the increase in focal length and lens order improves the resolution: when the design focal length is 25 mm, the lateral resolution is 1.2 mm, 1.16 mm and 1.08 mm respectively. When the design focal length is 50 mm, the lateral resolutions are 1.80 mm, 1.70mm and 1.64 mm respectively. The axial acoustic field distribution is illustrated in **Figure C3 (f)-(h)**, showing that the lens with a 50mm focal length achieves deeper focus than the 25mm lens, resulting in a longer imaging range along the axis.

Appendix C.3 Ultrasonic Imaging Test

Table C1 Specific dimensions of the USAF 1951 resolution test chart

line number	-2	-1	0	1	2	3
1	0.250	0.500	1	2	4	8
2	0.280	0.561	1.12	2.24	4.49	8.98
3	0.315	0.630	1.26	2.52	5.04	10.1
4	0.353	0.707	1.41	2.83	5.66	11.3
5	0.397	0.793	1.59	3.17	6.35	12.7
6	0.445	0.891	1.78	3.58	7.13	14.3

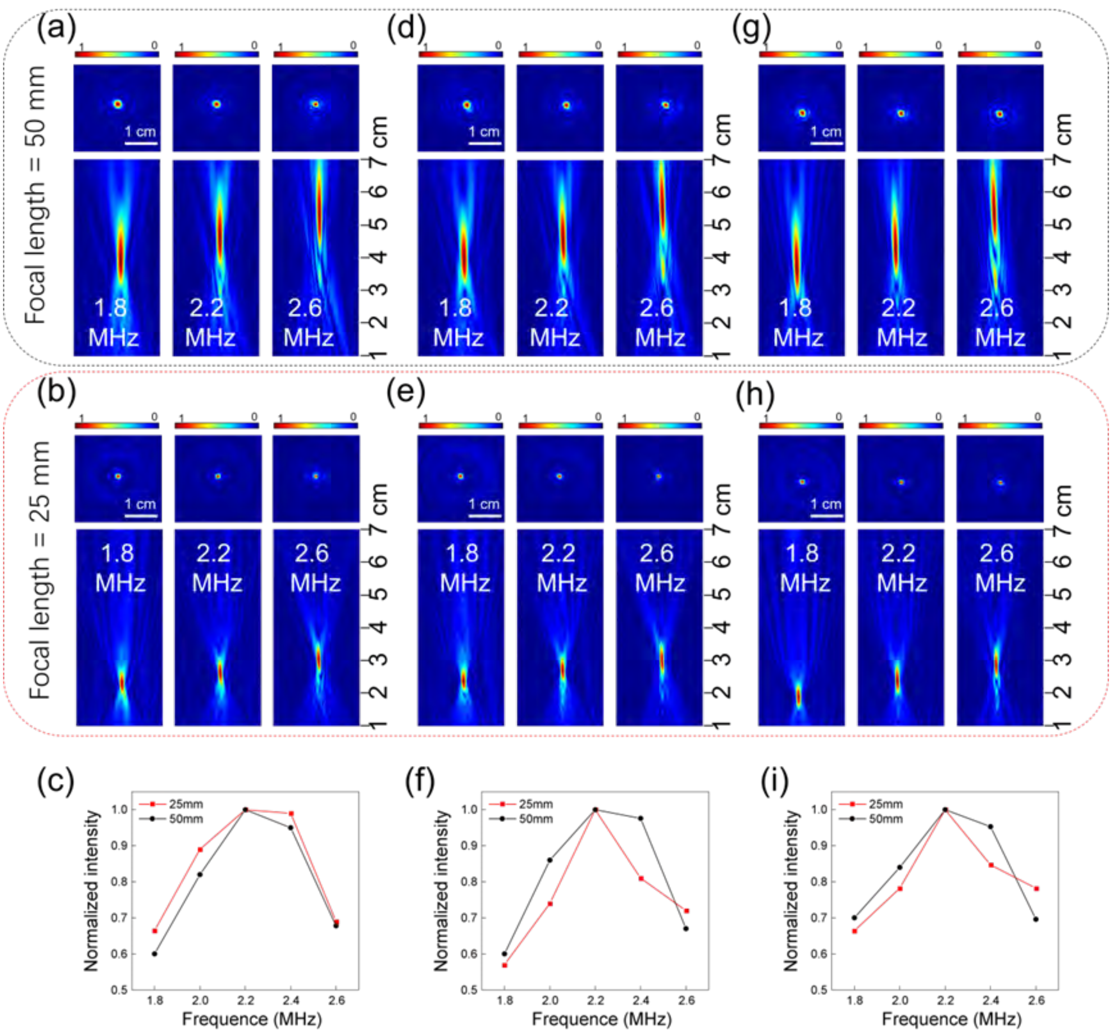

Figure C2 Acoustic field intensity maps for Fresnel lenses at 1.8 to 2.6 MHz, 25mm and 50mm focal lengths: (a), (b) fourth-order; (d), (e) sixth-order; (g), (h) eighth-order, showcasing x-y and x-z distributions respectively. The design focal length within the black dashed wireframe is 50 mm, while the design focal length within the red dashed wireframe is 25 mm. (c), (f), and (i) are the amplitude cross-sectional plots at the focal points of the 4th-order, 6th-order, and 8th-order Fresnel lenses at 1.8 to 2.6 MHz, respectively.

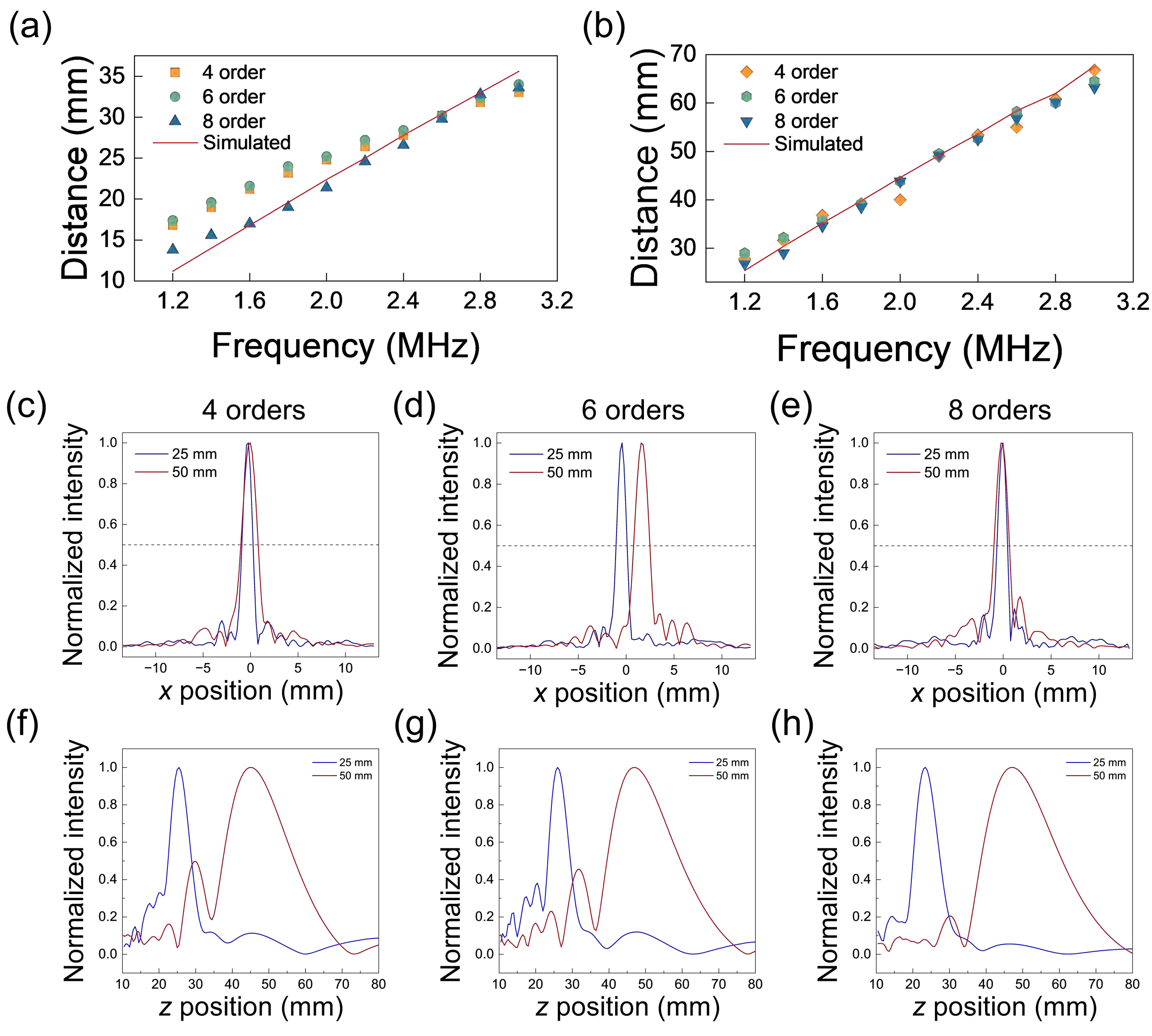

Figure C3 (a)-(b) Comparison of simulated and experimental focal length distribution for 1-3-2 piezoelectric composite transducer with different order Fresnel lenses at 25mm and 50mm. (c)-(e) Acoustic pressure distribution along the lateral central axis beyond the focal point for fourth, sixth, and eighth-order lenses, respectively. The axial acoustic field distribution is depicted in (f)-(h).

Appendix C.4 Parameter Performance Comparison

Table C2 COMPARISON OF PERFORMANCE OF THE ULTRASONIC TRANSDUCERS WITH FRESNEL LENS

Works	Piezoelectric Material	Frequency	Sensitivity	Bandwidth	Resolution	Focus length
This work	PZT5H/ Epoxy	2.2 MHz	2.4 V/275 V	20.07%	1.64-1.80 mm	50 mm
Mallay et al [8]	PZT5A/ Epoxy	5 MHz	36 mV/MPa	15%	0.34 mm	5.8 mm
Wang et al [9]	PZT4	5.46 MHz	60 mV/275 V	11.54%	0.6 mm	23.8-21.9 mm

References

1 T. Wei, H. Wang, and J. Su, "Research, design, and analysis of a stacked piezoelectric metamaterial structured sensitive element," J. Mater. Sci.: Mater. Electron., vol. 34, p. 1828, Sep. 2023, doi: 10.1007/s10854-023-11211-1.
2 S.H. Choy, H.L.W. Chan, M.W. Ng, and P.C.K. Liu, "Study of 1-3 PZT fibre/epoxy composite force sensor," Appl. Phys. A, vol. 81, pp. 817–821, Sep. 2005, doi: 10.1007/s00339-004-2874-9.
3 H. Dong, Z. Zhu, Z. Li, M. Li, and J. Chen, "Piezoelectric composites: State-of-the-art and future prospects," JOM, vol. 75, no. 1, pp. 340–352, 2023, doi: 10.1007/s11837-023-06202-w.
4 H. Wang, Y. Li, H. Hui, and T. Rong, "Analysis of electromechanical characteristics of the 1-3-2 piezoelectric composite and 1-3-2 modified structural material," Ceram. Int., vol. 48, no. 15, pp. 22323–22334, Aug. 2022, doi: 10.1016/j.ceramint.2022.04.238.
5 R. Lirette and J. Mobley, "Broadband wave packet dynamics of minimally diffractive ultrasonic fields from axicon and stepped fraxicon lenses," J. Acoust. Soc. Am., vol. 146, no. 1, p. 103, Jul. 2019, doi: 10.1121/1.5116011.
6 Y. Tang and E.S. Kim, "Simple sacrificial-layer-free microfabrication processes for air-cavity Fresnel acoustic lenses (ACFALs) with improved focusing performance," Microsyst. Nanoeng., vol. 8, p. 75, Jul. 2022, doi: 10.1038/s41378-022-00407-w.
7 K.A. Wear, "Hydrophone spatial averaging correction for acoustic exposure measurements from arrays—Part I: Theory and impact on diagnostic safety indexes," IEEE Trans. Ultrason. Ferroelectr. Freq. Control, vol. 68, no. 3, pp. 358–375, Feb. 2021, doi: 10.1109/TUFFC.2020.3037946.
8 M.G. Mallay, J.K. Woodacre, T.G. Landry, N.A. Campbell, and J.A. Brown, "A dual-frequency lens-focused endoscopic histotripsy transducer," IEEE Trans. Ultrason. Ferroelectr. Freq. Control, vol. 68, no. 9, pp. 2906–2916, Sep. 2021, doi: 10.1109/TUFFC.2021.3078326.
9 D. Wang, P. Lin, Z. Chen, C. Fei, Z. Qiu, Q. Chen, X. Sun, Y. Wu, and L. Sun, "Evolvable acoustic field generated by a transducer with 3D-printed Fresnel lens," Micromachines, vol. 12, no. 11, p. 1315, Oct. 2021, doi: 10.3390/mi12111315.